

Extracellular matrix remodelling is associated with muscle force increase in overloaded mouse *plantaris* muscle

A. Stantzou* , K. Relizani*[†] , S. Morales-Gonzalez[†] , C. Gallen*, A. Grassin*, A. Ferry[‡]§, M. Schuelke[†]  and H. Amthor*^{***} 

*Université Paris-Saclay, UVSQ, Inserm, END-ICAP, Versailles, France, [†]NeuroCure Cluster of Excellence and Department of Neuropediatrics, Charité-Universitätsmedizin Berlin, Corporate member of the Freie Universität Berlin and Humboldt-Universität zu Berlin, and Berlin Institute of Health, Berlin, Germany, [‡]Center for Research in Myology, Pierre et Marie Curie University, Paris Sorbonne, INSERM, UMRS974, CNRS FRE3617, Paris, France, [§]Université Paris Descartes, Sorbonne Paris Cité, Paris, France and ^{***}Charité - Universitätsmedizin Berlin, Charitéplatz 1, 10117, Berlin

A. Stantzou, K. Relizani, S. Morales-Gonzalez, C. Gallen, A. Grassin, A. Ferry, M. Schuelke and H. Amthor (2021) *Neuropathology and Applied Neurobiology* 47, 218–235

Extracellular matrix remodelling is associated with muscle force increase in overloaded mouse *plantaris* muscle

Aims: Transforming growth factor- β (TGF- β) signalling is thought to contribute to the remodelling of extracellular matrix (ECM) of skeletal muscle and to functional decline in patients with muscular dystrophies. We wanted to determine the role of TGF- β -induced ECM remodelling in dystrophic muscle. **Methods:** We experimentally induced the pathological hallmarks of severe muscular dystrophy by mechanically overloading the *plantaris* muscle in mice. Furthermore, we determined the role of TGF- β signalling on dystrophic tissue modulation and on muscle function by (i) overloading myostatin knockout (*Mstn*^{-/-}) mice and (ii) by additional pharmacological TGF- β inhibition *via* halofuginone. **Results:** Transcriptome analysis of overloaded muscles revealed upregulation predominantly of genes associated with ECM, inflammation and metalloproteinase activity.

Histology revealed in wild-type mice signs of severe muscular dystrophy including myofibres with large variation in size and internalized myonuclei, as well as increased ECM deposition. At the same time, muscle weight had increased by 208% and muscle force by 234%. Myostatin deficiency blunted the effect of overload on muscle mass (59% increase) and force (76% increase), while having no effect on ECM deposition. Concomitant treatment with halofuginone blunted overload-induced muscle hypertrophy and muscle force increase, while reducing ECM deposition and increasing myofibre size. **Conclusions:** ECM remodelling is associated with an increase in muscle mass and force in overload-modelled dystrophic muscle. Lack of myostatin is not advantageous and inhibition of ECM deposition by halofuginone is disadvantageous for muscle plasticity in response to stimuli that induce dystrophic muscle.

Keywords: fibrosis, overload, muscular dystrophy, muscle force, myostatin, halofuginone, TGF- β , array-based transcriptome analysis

Correspondence: Helge Amthor, Laboratoire Biothérapie des Maladies du Système Neuromusculaire, UFR Simone Veil – Santé, Université de Versailles Saint-Quentin-en-Yvelines, 2 avenue de la Source de la Bièvre, 78180 Montigny-Le-Bretonneux, France. Tel.: +33 1 70 42 92 29; E-mail: helge.amthor@uvsq.fr

Markus Schuelke, Department of Neuropediatrics, Charité – Universitätsmedizin Berlin, Augustenburger Platz 1, 13353 Berlin, Germany. Tel: +49 30 4505 66112, Fax: +49 30 4505 66920; E-mail: markus.schuelke@charite.de

[Correction added on 11 March 2021, after first online publication: [Charité - Universitätsmedizin Berlin was added for H. Amthor.]

Introduction

Muscle fibrosis, histologically observable by an increased deposition of extracellular matrix (ECM) proteins, is a hallmark of muscular dystrophy; however, its functional consequence is largely unknown. The increase in muscle connective tissue can be accompanied by an increase in muscle mass at initial stages of disease, such as typically seen in the calf muscles of boys with Duchenne muscular dystrophy (DMD). Muscle hypertrophy is associated with a larger absolute muscle force in the *mdx* mouse model of DMD [1,2]. However, human DMD muscle, in contrast to *mdx* mouse muscle, eventually exhibits irreversible muscle wasting and becomes paralytic due to fatty-fibrotic metaplasia. The pathophysiological events leading to the histological changes of fibrosis in muscular dystrophies are well known. Muscle fibres destabilize at the sarcolemmal level due to the lack of specific proteins in the dystrophin-associated glycoprotein complex, for example, dystrophin in the case of DMD. Destabilized fibres are prone to contraction-induced damage and necrosis, which in turn induces inflammation, macrophage-induced clearance of degenerated fibres, muscle stem cell activation and myofibre regeneration. However, macrophages as well as regenerating muscle stimulate so-called fibro/adipogenic precursors (FAPs), which are the main ECM producing myofibroblasts in skeletal muscle [3,4]. Following repetitive cycles of de- and regeneration and ensuing permanent ECM production, skeletal muscle of DMD patients degrades entirely towards fatty fibrosis at the end stage [5–7]. Chronic cycles of muscle de- and regeneration alters molecular signature of FAPs, which become primed towards a fibroblast fate under TGF- β signalling, whereas acquired insensitivity to Notch signalling directs FAPs towards an adipocyte fate [8,9]. The pathogenic response of FAPs depends also on the type of muscular dystrophy. Indeed, in the *mdx* mouse, FAPs shift to persistent fibrogenesis, whereas in the mouse model for limb muscular dystrophy type 2B, FAPs cause adipogenic muscle replacement [8,10].

Current concepts consider connective tissue stimulation as an epiphenomenon of muscle de- and regeneration caused by associated inflammation [11]. Manifest fibrosis is thought to have a negative feedback on muscle regeneration, as it coincides in time with the

gradual disappearance of muscle fibres [7]. In DMD patients, muscle becomes stiffer from early disease stages onwards, eventually leading to musculo-tendinous retraction. In DMD, fibrosis is initially more advanced at the level of the muscle-tendon interphase [12], suggesting a heterogeneous response to pathophysiological stimuli along the length of the muscles and a regional specificity of ECM function.

Increased ECM deposition and muscle fibrosis are commonly regarded as pathogenic events that would call for therapeutic intervention [13,14]. Several of such interventions with antifibrotic agents interfering with TGF- β signalling have been tested in hundreds of patients with muscular dystrophy since 2005. However, they show a lack of efficacy in those trials for which results are available, whereas many trials are not yet concluded (NCT02525302; NCT01978366; NCT01847573; NCT02515669; NCT02310763; NCT02907619; NCT02841267; NCT02606136; NCT02354781; NCT01239758; NCT01099761; NCT01519349 and NCT00104078).

TGF- β signalling, notably *via* growth factors TGF- β 1 and myostatin, strongly stimulates muscle fibrosis by an increase in intracellular Smad2/3 activity and subsequent ECM synthesis and remodelling [11,15]. Inhibition of TGF- β signalling by neutralizing antibodies directed against TGF- β 1 or TGF- β -receptor 1 reduces muscle fibrosis and increases muscle regeneration [16,17]. Abrogation of myostatin signalling either in *Mstn*^{-/-} mice or by treatment with soluble activin receptor-IIb decreased fibrosis and increased muscle regeneration [18–20]. Halofuginone blocks TGF- β -mediated collagen synthesis through inhibition of Smad3 phosphorylation [21]. In the *mdx* mouse, halofuginone decreases muscle fibrosis, increases muscle stem cell activity and increases muscle fibre size, thereby exerting an antidystrophic effect [22–26].

In normal mice, chronic mechanical overload of the *plantaris* muscle can elicit histological hallmarks of muscular dystrophy. In an experimental setting, this can be achieved by surgical ablation of synergic muscles [27–31]. Such mechanical stress causes muscle degeneration and inflammation in the beginning, followed by regeneration, increased variation in myofibre size with an increase in mean fibre cross-sectional area and increased ECM deposition, resulting in increased

muscle mass [32–38]. Strikingly, this tissue adaptation causes an increase in maximal tetanic force of up to 100% [30,36]. Presently, researchers think this force increase would be the result of muscle fibre hypertrophy only.

We here interfered with TGF- β signalling during the adaptive response of the *plantaris* muscle following surgical ablation of synergic muscles. We tested the effect of halofuginone treatment on muscle physiology and on the muscle transcriptome in the overloaded muscles. We found, rather surprisingly, that an increase in muscle force indeed requires TGF- β -mediated ECM remodelling, whereas muscle fibre hypertrophy itself seems to be dispensable.

Methods

Animals, mechanical overloading and treatment

We performed all procedures in accordance with national and European legislation, under the license 75-1102 (France). Three-month-old female *Mstn*^{-/-} (n = 6) mice [39] and age- and sex-matched wild-type (*WT*) control mice (n = 6) of the same genetic background (C57BL/6J) were used for this study. For morphometric and transcriptomic analysis of overloading, animals were anesthetized with intraperitoneal pentobarbital (50 mg/kg body weight) and the *plantaris* muscles on both sides were mechanically overloaded by surgical removal of the *soleus* muscles and of a major portion of the *gastrocnemius* muscles as described [19,27]. After 2 weeks of overloading, mice were sacrificed by atlanto-occipital dislocation for removal and cryopreservation of both *plantaris* muscles. For investigation of pharmacological TGF- β -inhibition, *Mstn*^{-/-} (n = 6) and control mice (n = 6) were injected three times per week for 6 weeks intraperitoneally with either 10 μ g of halofuginone (Vetranal[®], SIGMA 32481) or the equivalent volume of PBS. We started the identical overload procedure 2 weeks after initiation of the halofuginone treatment and measured muscle force of the *plantaris* muscle 5 weeks later. After sacrifice, we dissected and cryopreserved the *plantaris* muscle for histological analysis.

Whole muscle force measurements

Skeletal muscle function was evaluated by measuring *in situ* isometric force, as previously described [36].

Animals were anaesthetized as described above. During the physiological experiments, supplemental doses were given as required to maintain deep anaesthesia. The knee and foot were fixed with clamps and stainless-steel pins. The *plantaris* muscle was exposed and the distal tendon was cut and attached to an isometric transducer (Harvard Bioscience, Holliston, MA, USA) using a silk ligature. The sciatic nerves were proximally crushed and distally stimulated with a bipolar silver electrode using supramaximal square-wave pulses of 0.1 ms duration. Responses to tetanic stimulation with a pulse frequency of 50–143 Hz were recorded during successive bursts. At least 1 min was allowed between the trains of contractions. Absolute maximal force was determined at the optimal length, being considered the length of the muscle at which maximal tension was obtained during the tetanus. Force was normalized to the muscle mass as an estimate of specific maximal force. Body temperature was maintained at 37°C using radiant heat throughout the experiment.

Histology

Serial transverse sections of 12 μ m from *plantaris* muscles from the mid-belly region were obtained using a cryostat. Haematoxylin and eosin staining was performed using routine histological protocols. For MHC immunohistochemistry, frozen unfixed 12 μ m sections were blocked for 1 h in PBS containing 2% BSA and 2% foetal calf serum. Sections were then incubated overnight with primary antibodies. After washes in PBS, sections were incubated for 1 h with secondary antibodies with various fluorophores (Alexa Fluor[®], ThermoFisher Scientific, Waltham, MA, USA). After washes in PBS, slides were finally mounted with Fluoromount-G (ThermoFisher Scientific). For expression analysis of myosin heavy-chain (MHC) isoforms we used as primary antibodies: anti-MHCI (hybridoma#A4.840, DSHB), anti-MHCIIa (hybridoma#SC-71, DSHB) and anti-MHCIIb (hybridoma#BF-F3, DSHB). Other primary antibodies were anti-laminin (Z0097, Agilent Dako, Santa Clara, CA, USA) and anti-collagen 1 (ab34710, Abcam, Cambridge, UK).

For the quantification of collagen-1 fluorescence intensity on full cross sections of the *plantaris* muscle, all parameters during image acquisition were kept identical and the images were analysed morphometrically for the percentage of collagen per muscle cross section

after identical grey-level thresholding using ImageJ v1.49 (<https://imagej.nih.gov/ij/>).

Muscle fibre morphology was also investigated on full cross sections of the *plantaris* muscle. Images were captured using a digital camera (Hamamatsu ORCA-AG, Massy, France) attached to a motorized fluorescence microscope stage (Zeiss AxioImager Z1, Jena, Germany). These images were projected onto a flat-screen coupled with a graphic tablet that enabled manual retracing of muscle fibre outlines. Morphometric analyses were done with the MetaMorph v7.5 software (Molecular Devices, Sunnyvale, California, USA).

Transcriptome analysis

Frozen muscle was homogenized on ice using an ultraturax (15951-45; IKA, Staufen, Germany) and RNA was extracted *via* the TRIzol® protocol. $N = 6$ samples of each condition were analysed (3 animals, both legs). Quality of the RNA was controlled using the 2100 Bioanalyzer (Agilent, Santa Clara, CA, USA). cRNA was produced, labelled and hybridized, according to the manufacturer's instructions, on the GeneChip® Mouse Gene 1.0 ST Array (Affymetrix, Santa Clara, CA, USA), which represents 28,853 genes; 27,543 with ENSEMBL support and 19,434 with full-length RefSeq support. The arrays were scanned with the 428 Scanner (Affymetrix) and signal intensities were processed with the Affymetrix GeneChip Command Console Software (AGCC) to produce the RMA (Robust Multi-Array Average) normalized CEL files that could be uploaded to the GenePattern platform for further downstream analysis and visualization [40].

We identified those genes that were significantly up- and downregulated between the various conditions by at least a factor of 2.0. In order to control for multiple testing, we only considered genes as significantly regulated if their false discovery rate (FDR) was below 0.01. The raw data of this experiment can be accessed at the GEO database under GSE127255, URL: <https://www.ncbi.nlm.nih.gov/geo/query/acc.cgi?acc=GSE127255>. Pathway, gene network and functional annotation analysis of the regulated genes were done with DAVID 6.8 at the URL: <https://david.ncifcrf.gov/term2term.jsp> using the default settings [41]. Enrichment of gene clusters was considered significant if the FDR was below 0.01. For Principal Component Analysis in two dimensions (PCA 2D), we $\ln(x)$ -transformed the original

values and applied the unit variance scaling to rows. We calculated the principal components by singular value decomposition (SVD) with imputation using the program ClustVis at <https://biit.cs.ut.ee/clustvis/> [42]. The exact list of genes and their expression differences is provided in Table S1.

RNA isolation and RT-qPCR

Total RNA from frozen *plantaris* muscle tissue was isolated using TRIzol® (ThermoFisher Scientific) extraction in combination with the RNeasy Mini kit (Qiagen, Hilden, Germany). RNase-free DNase I (Qiagen or ThermoFisher Scientific) was used to eliminate traces of DNA in the RNA extract. Isolated RNA was quantified using the NanoVue Plus GE HealthCare spectrophotometer (Dutscher, Issy-les-Moulineaux, France). cDNA synthesis was done on full RNA extracts from muscle using the ThermoScript RT-PCR system (ThermoFisher Scientific) with random hexamer primers for first-strand cDNA synthesis. Reverse transcription quantitative polymerase chain reaction (RT-qPCR) was done according to the SYBR Green protocol (BioRad, Hercules, CA, USA) in triplicates on the CFX96 Touch Real-Time detection system (BioRad) using iTaq Universal SYBR Green Supermix (BioRad). A 10 min denaturation step at 94°C was followed by 40 cycles of denaturation at 94°C for 10 s and annealing/extension at 60°C for 30 s. Before sample analysis, we had determined for each gene and primer set the PCR efficiencies with a standard dilution series (10E1-10E7 copies/ μ l), which subsequently enabled us to determine the copy numbers from the C_t values. mRNA levels were normalized to 10E3 copies of *Gapdh* mRNA or 10E6 copies 18S rRNA. Fold changes were calculated according to the efficiency corrected $-\Delta\Delta C_t$ method [43]. The sequences for the oligonucleotide primers are listed in Table S2.

Statistical analysis

We compared groups statistically using the ANOVA test, except as for comparing fibre diameters, for which we used the two-tailed non-parametric Mann-Whitney U-Test because of high n-number. Values are depicted as means \pm SD (Standard Deviation). Significance levels were set at $P < 0.05$. For transcriptome analysis and for other multiple testing procedures, results were

considered significant if the False Discovery Rate (FDR) was below 0.01 [44].

Results

Part 1: Determination of the molecular signature of overload

We performed an array-based transcriptome analysis after 2 weeks of *plantaris* muscle overloading. This provided a global view on cellular processes during muscle adaptation to overload. The investigated muscles fell into four groups: (i) untreated wild-type (*WT*) muscle; (ii) overloaded wild-type (*WT-OVL*) muscle; (iii) untreated myostatin knockout (*Mstn*^{-/-}) muscle and (iv) overloaded myostatin knockout (*Mstn*^{-/-}-OVL) muscle.

Comparison of transcriptome signatures between *WT* and *WT-OVL* muscles

In *WT* mice, overload caused a significant upregulation by a factor of 2.0 or above of $n = 909$ genes and downregulation of $n = 342$ genes (Table S1). Functional clustering revealed that the highest enrichment scores for Gene Ontology (GO) terms were associated with the ECM, inflammation and metalloproteinase activity as a strong indicator of ECM remodelling (Figures 1 and 2A). Interestingly, the highest GO-term depletion scores were mainly associated with muscle metabolic function such as mitochondrial metabolism, glycogen usage and oxidoreductase activity (Figures 1 and 3A).

Comparison of mRNA expression levels of ECM genes between *WT* and *Mstn*^{-/-} muscles

Transcriptome and cluster analysis of ECM genes did not reveal any difference between untreated *WT* and *Mstn*^{-/-} muscles (Figure 2A). Remarkably, on two-dimensional principal component analysis (PCA 2D), individual muscles from both genotypes clustered very closely and both groups largely overlapped. This suggests little interindividual variability and near equal ECM gene expression in both genotypes. Overload induced strong upregulation of the entire ECM gene cluster in both genotypes. However, now the PCA 2D blot reveals a clear separation between the two

genotypes with a comparatively higher upregulation of ECM genes in the *WT* group. This suggests that lack of myostatin, as expected, would reduce ECM remodelling via attenuation of the TGF- β signalling pathway activation, albeit not completely abrogating it by far.

We next confirmed the results of RNA-microarray analysis by RT-qPCR for representative up- and down-regulated genes. We found that mRNA copy number fold changes correlated between RNA sequencing and RT-qPCR for all analysed genes including exemplary ECM-associated genes *Postn*, *Mmp12* and *Col6a3* (Figure S1).

Comparison of mRNA expression levels of inflammatory response genes between *WT* and *Mstn*^{-/-} muscles

Transcriptome and cluster analysis of inflammatory response genes again revealed little differences between untreated *WT* and *Mstn*^{-/-} muscles (Figure 2B). However, overload induced a strong inflammatory response in both genotypes, with a large overlap of both muscle groups on the PCA 2D blot, suggesting that lack of myostatin did not protect from overload-induced myofibre necrosis and its subsequent inflammatory response.

Comparison of mRNA expression levels of genes encoding mitochondrial proteins between *WT* and *Mstn*^{-/-} muscles

RNA expression analysis and cluster analysis for genes encoding mitochondrial proteins revealed similar sets of high- and low-expressing genes, if comparing untreated *WT* and *Mstn*^{-/-} muscles following unit variance scaling (Figure 3A). However, the magnitude of expression differed between the two genotypes, resulting in a clear separation of the genotypes along the ordinate of the PCA 2D blot. Overload moved gene expression in the same direction, however, with lesser response in *Mstn*^{-/-}-OVL.

Comparison of mRNA expression levels of genes encoding sarcomeric proteins between *WT* and *Mstn*^{-/-} muscles

Transcriptome and cluster analysis of genes encoding sarcomeric proteins revealed an entirely different

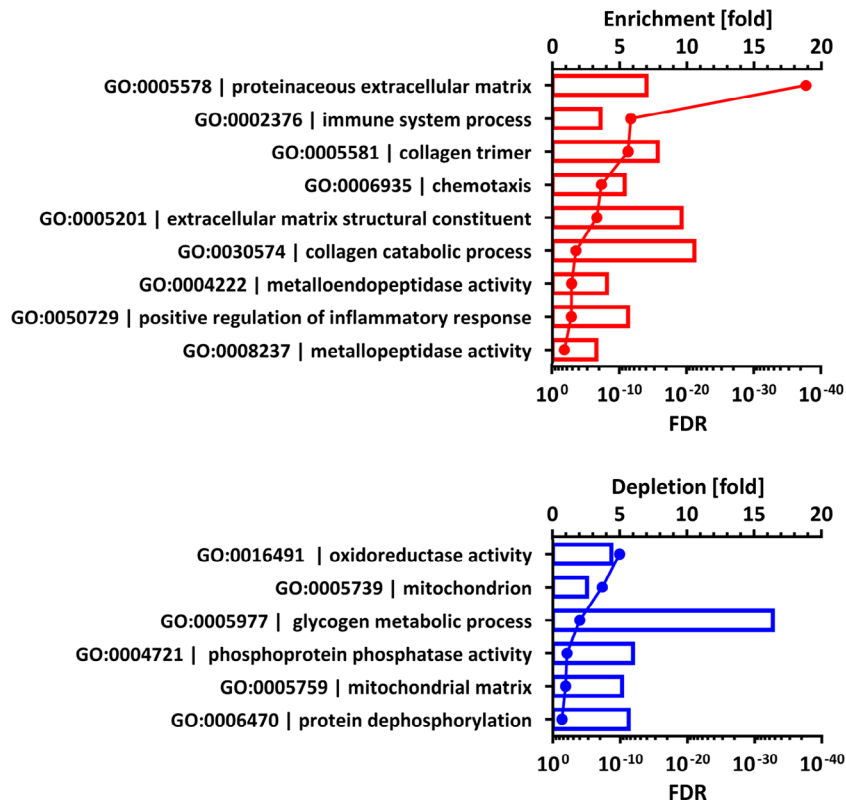


Figure 1. Relative enrichment and depletion of muscle expressed genes after overload. *WT* and *Mstn*^{-/-} samples were combined. The bars depict the relative fold enrichment or depletion of groups of GO-annotated genes, while the dots depict the false discovery rate (FDR). All enrichments and depletions were significant with an FDR < 0.01.

expression status between untreated *WT* and *Mstn*^{-/-} muscles (Figure 3B), thereby confirming previous data following Affymetrix GeneChip analysis [45]. Furthermore, overload changed gene expression profiles in both genotypes, however, clusters remained separated when comparing the groups on the PCA 2D blot. This suggests that the contractile phenotype of skeletal muscle adapts differently to overload in the absence of myostatin.

We next analysed transcription of genes encoding muscle myosin isoforms (Figure S2). We found a clear separation of gene clusters on the PCA 2D blot depending on the genotype (*Mstn*^{-/-} versus *WT*) and whether muscles were overloaded or not. The clustergram allowed us to compare the expression of an exemplary set of genes characteristic for oxidative and glycolytic muscle fibres. As expected, *WT* muscle expressed *Myh2* and *Myh7* encoding oxidative isoforms (MHC2a and MHC1, respectively), whereas both were downregulated in untreated *Mstn*^{-/-} muscle. Furthermore, during

overload we observed a downregulation of *Myh4* in *WT* muscle, encoding the fast glycolytic isoform (MHC2b), which was consistent with a fibre conversion towards oxidative isoforms. However, *Mstn*^{-/-} muscle failed to downregulate the glycolytic isoform and to upregulate oxidative isoforms in response to overload, suggesting that *Mstn*^{-/-} muscle may resist overload-induced fibre type conversion.

Of note, overload-induced expression of developmental MHC isoforms *Myh3* (encoding embryonic MHC), *Myh8* (encoding perinatal MHC) and *Myh4* (encoding embryonic MLC1) was seen in both genotypes. This finding is in line with an overload-induced degeneration/regeneration cycle and the emergence of myofibres with internalized myonuclei (see below).

Part 2: Tissue and functional response to overload

Our RNA expression analysis suggested ECM remodelling to be a significant adaptive response of muscle to

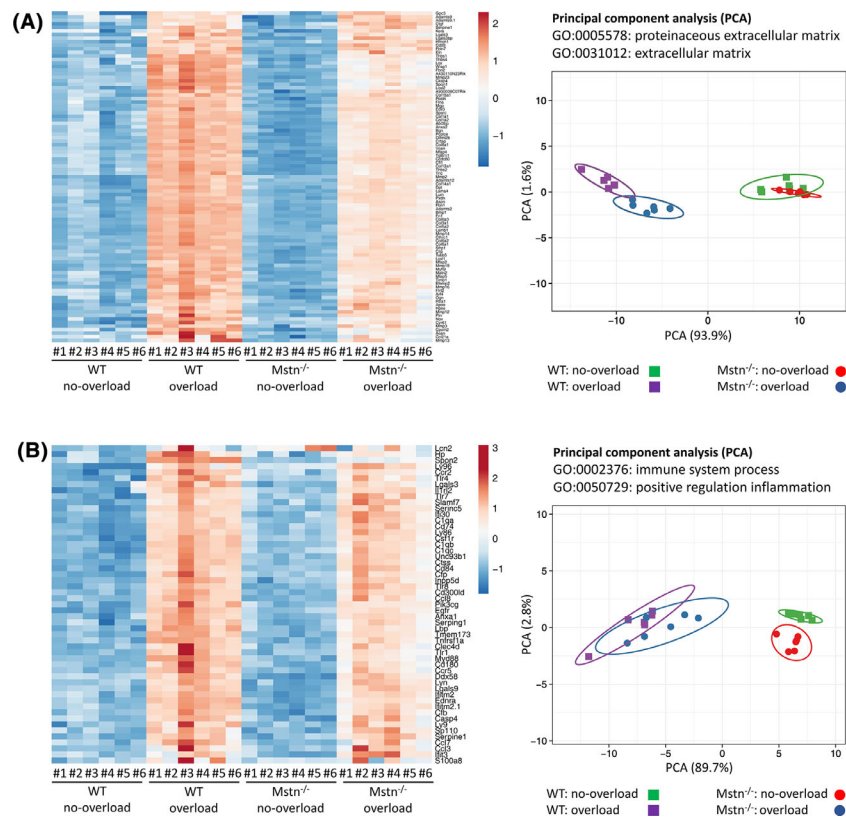


Figure 2. Relative regulation after overload of transcript numbers of genes associated with the extracellular matrix and the immune system in the muscle of WT and *Mstn*^{-/-} mice. (A) Heat map and clustergram of the genes associated with the GO-terms *proteinaceous extracellular matrix* (GO:0005578) and *extracellular matrix* (GO:0031012). (B) Heat map and clustergram of the genes associated with the GO-terms *immune system process* (GO:0002376) and *positive regulation of inflammatory response* (GO:0050729). For both systems, the up-regulation was more prominent in the WT samples as compared to the *Mstn*^{-/-} muscle samples. The Principal Component Analysis in two dimensions (PCA 2D) of the four experimental conditions with six biological replicates is depicted on the right side. For PCA 2D, original values were ln(x)-transformed and the unit variance scaling was applied to rows; singular value decomposition (SVD) with imputation was used to calculate principal components. X- and Y-axes show principal components 1 and 2 that explain the indicated total variance. Prediction ellipses are such that with probability 0.95, a new observation from the same group will fall inside the ellipse. N = 24 data points. The exact list of genes and their expression differences is provided in Table S1.

overload. We next wanted to understand the consequence of overload-induced ECM remodelling on muscle structure and function. In addition, our RNA expression studies suggested, rather surprisingly, that myostatin abrogation did not prevent muscle fibrosis. Hence, we additionally treated WT and *Mstn*^{-/-} mice with the fibrosis inhibitor halofuginone.

Plantaris muscles from sedentary adult WT and *Mstn*^{-/-} mice were subjected to 5 weeks of mechanical overload following surgical ablation of *soleus* and *gastrocnemius* muscles. Animals were concomitantly treated with either halofuginone or PBS, starting 2 weeks before the surgical intervention. We thus obtained muscles from eight different experimental settings: (i)

control wild-type PBS injected (WT-PBS); (ii) overload wild-type PBS injected (WT-OVL-PBS); (iii) halofuginone treated wild-type (WT-HLF); (iv) overload and halofuginone-treated wild-type (WT-OVL-HLF); (v) control myostatin knockout PBS injected (*Mstn*^{-/-}-PBS); (vi) overload myostatin knockout (*Mstn*^{-/-}-OVL-PBS); (vii) halofuginone-treated myostatin knockout (*Mstn*^{-/-}-HLF); (viii) overload and halofuginone-treated myostatin knockout (*Mstn*^{-/-}-OVL-HLF).

Effect of overload on muscle ECM remodelling

Quantification of muscle cross-section area (CSA) occupied by collagen 1 expression revealed an increase from

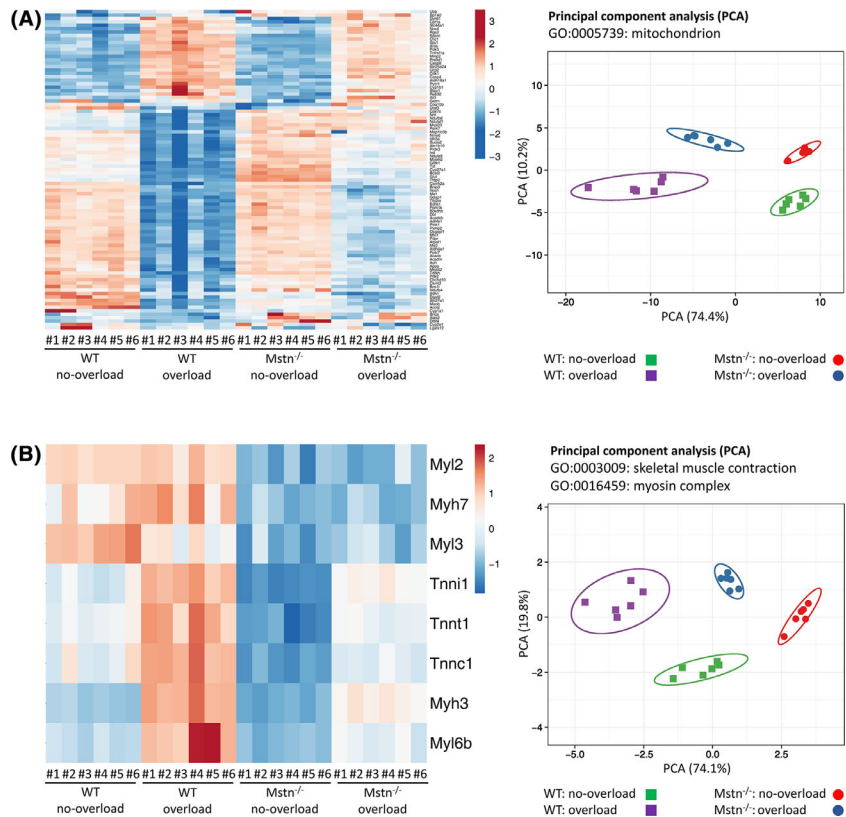


Figure 3. Relative regulation after overload of transcript numbers of genes associated with the mitochondrion and structural proteins of the skeletal muscle in WT and *Mstn*^{-/-} mice. (A) Heat map and clustergram of the genes associated with the GO-term *mitochondrion* (GO:0005739). (B) Heat map and clustergram of the genes associated with the GO-terms *skeletal muscle contraction* (GO:0003009), *ventricular cardiac muscle tissue morphogenesis* (GO:0055010), *transition between fast and slow fibre* (GO:0014883), *myosin complex* (GO:0016459), *cardiac muscle contraction* (GO:0060048) and *troponin complex* (GO:0005861). The PCA 2D of the four experimental conditions with six biological replicates is depicted on the right side. The exact list of genes and their expression differences are provided in Table S1.

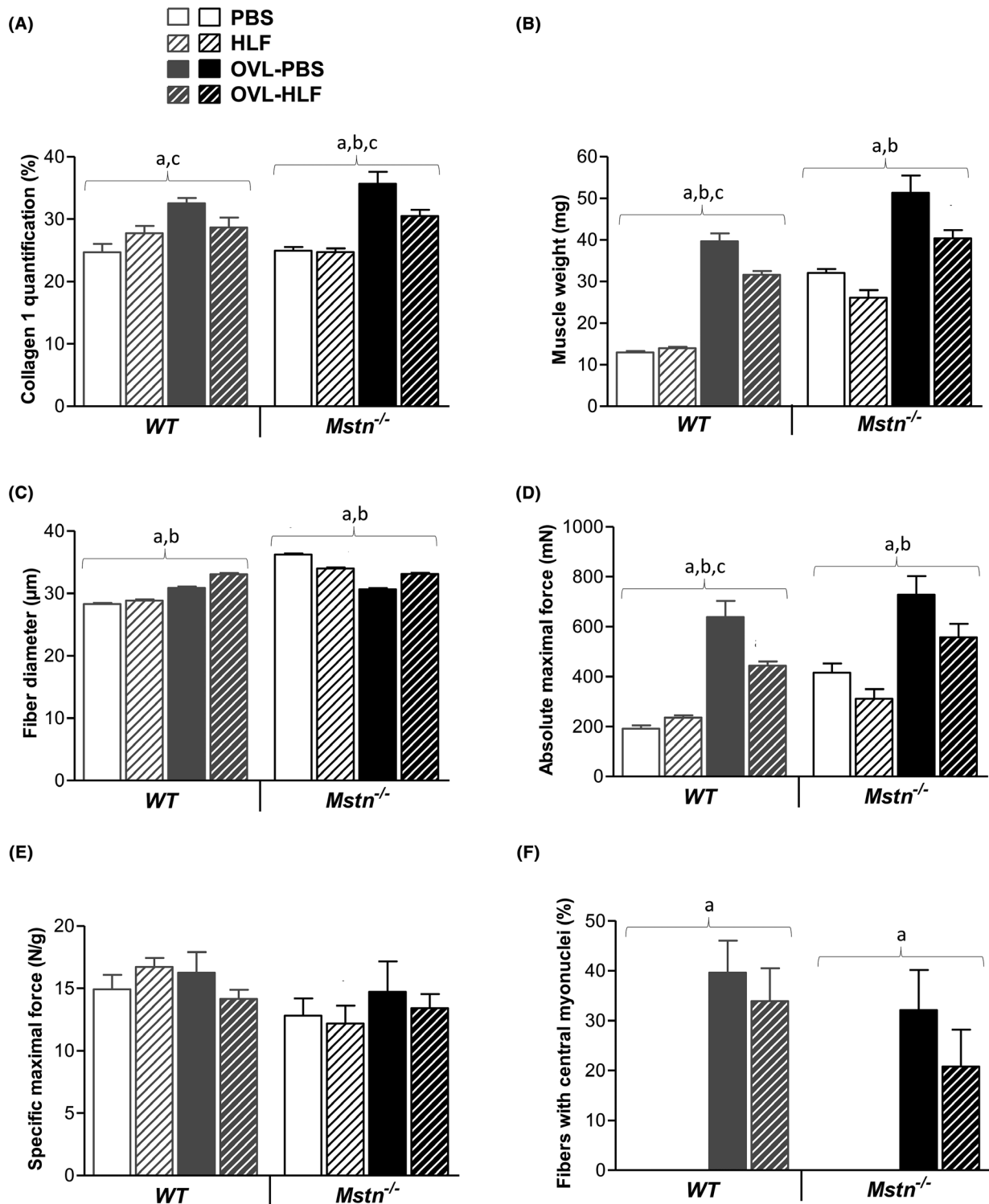
25% to 33% in WT-OVL *plantaris* muscle ($P = 0.0015$) and an increase from 25% to 36% in *Mstn*^{-/-}-OVL *plantaris* muscle ($P < 0.0001$), (Figures 4A and 5C). Concomitant treatment with halofuginone limited ECM deposition to 29% in WT-OVL-HLF ($P = 0.0102$), thus 4% less than in WT-OVL (29% compared to 33%) and limited increase to 31% in *Mstn*^{-/-}-OVL-HLF ($P = 0.0311$), thus 5% less than in *Mstn*^{-/-}-OVL (31% compared to 36%). These results show that halofuginone, but not lack of myostatin, inhibited overload-induced ECM deposition.

Effect of overload on muscle mass

Overload induced a 208% weight increase in WT-OVL *plantaris* muscle (from an average of 13 to 40 mg,

$P < 0.0001$) and only 59% weight increase in *Mstn*^{-/-}-OVL *plantaris* muscle (from 32 to 51 mg, $P < 0.0001$), (Figure 4B). Concomitant halofuginone treatment restricted increase in muscle weight to 146% in WT-OVL-HLF ($P < 0.0001$), thus, 62% less than in WT-OVL (32 mg compared to 40 mg), and restricted increase to 25% in *Mstn*^{-/-}-OVL-HLF ($P = 0.0015$ for HLF effect, however, $P =$ non-significant for combined effect), thus, 34% less than in *Mstn*^{-/-}-OVL (40 mg compared to 51 mg).

Morphometric analysis (Figures 4C and 5A,B) revealed that overload increased fibre diameters by 11% in WT-OVL *plantaris* muscle (from 28 to 31 μm). Concomitant treatment with halofuginone increased fibre diameters further by 7% WT-OVL-HLF compared to WT-OVL (33 μm versus 31 μm). Strikingly, overload



completely abolished the hypertrophic effect of myostatin knockout and reduced fibre diameter by 14% in *Mstn*^{-/-}-OVL *plantaris* muscle (from 36 to 31 µm).

Concomitant treatment with halofuginone increased fibre diameter by 6% in *Mstn*^{-/-}-OVL-HLF in comparison to *Mstn*^{-/-}-OVL (33 µm versus 31 µm). Thus,

Figure 4. Effect of overload on muscle weight and force in *WT* and *Mstn*^{-/-} mice following halofuginone treatment. Adult female *WT* and *Mstn*^{-/-} mice were treated three times per week with intraperitoneal injections of PBS or 10 µg of halofuginone (HLF) for 6 weeks. Overload (OVL) surgery on the *plantaris* muscle was done after 2 weeks of treatment on both hind limbs. Mice were analysed 5 weeks after the overload surgery. *WT* diagrams are in grey, *Mstn*^{-/-} diagrams are in black. Values are depicted as means ± SD. (A) Diagrams depict the percentage of cross-sectional area positive for the collagen 1 immune signal at mid-belly cross sections of the *plantaris* muscle (n = 9-15). Significance levels were calculated using the two-way ANOVA test. *WT* diagram: ^aP = 0.0015 (effect of OVL), ^cP = 0.0102 (combined effect of OVL and HLF). *Mstn*^{-/-} diagram: ^aP < 0.0001 (effect of OVL), ^bP = 0.019 (effect of HLF) and ^cP = 0.0311 (combined effect of OVL and HLF). (B) Diagrams depict *plantaris* muscle wet weight (n = 6-12). Two-way ANOVA test was performed. *WT* diagram: ^aP < 0.0001 (effect of OVL), ^bP = 0.0011 (effect of HLF) and ^cP < 0.0001 (combined effect of OVL and HLF). *Mstn*^{-/-} diagram: ^aP < 0.0001 (effect of OVL) and ^bP = 0.0015 (effect of HLF). (C) Mean fibre diameter of the *plantaris* muscle fibres on mid-belly sections following immunostaining against collagen 1 (n = 2,000-5,000/group). Two-tailed non-parametric Mann-Whitney U-Test was performed. *WT* diagram: ^aP < 0.0001 (effect of OVL) and ^bP < 0.0001 (effect of HLF). *Mstn*^{-/-} diagram: ^aP < 0.0001 (effect of OVL) and ^bP < 0.0001 (effect of HLF). (D) Diagrams depict absolute maximal force. (n = 4-12/group). Two-way ANOVA test was performed. *WT* diagram: ^aP < 0.0001 (effect of OVL), ^bP = 0.0388 (effect of HLF) and ^cP = 0.0015 (combined effect of OVL and HLF). *Mstn*^{-/-} diagram: ^aP < 0.0001 (effect of OVL) and ^bP = 0.0224 (effect of HLF). (E) Diagrams depict *plantaris* muscle-specific maximal force (n = 4-12/group). Two-way ANOVA test revealed no statistical differences between groups. (F) Diagrams depict the percentage of fibres of the *plantaris* muscle containing at least one central myonucleus. Sections were quantified on mid-belly sections following haematoxylin and eosin staining (n = 3/group). Two-way ANOVA test was performed. *WT* diagram: ^aP < 0.0001 (effect of OVL). *Mstn*^{-/-} diagram: ^aP < 0.0001 (effect of OVL).

overload resulted in exactly the same fibre size (31 µm) irrespective of the genotype, which caused *WT* fibres to hypertrophy and *Mstn*^{-/-} fibres to hypotrophy. Concomitant halofuginone increased fibre diameter to 33 µm in both genotypes. All treatment effects on fibre diameter were highly significant ($P < 0.00001$).

In conclusion, these results suggest that the increase in muscle mass in response to overload is mainly due to an increase in ECM.

Effect of overload on muscle force generation

Overload induced a 234% increase in absolute maximal muscle force in *WT*-OVL *plantaris* (from 191 to 638 mN, $P < 0.001$), whereas it increased only by 132% under concomitant halofuginone treatment ($P = 0.0015$), thus, 102% less than in *WT*-OVL (444 mN versus to 638 mN) (Figure 4D). Remarkably, overload induced only a 76% force increase in *Mstn*^{-/-}-OVL *plantaris* (from 415 to 729 mN, $P < 0.0001$) (Figure 4D). Concomitant treatment with halofuginone limited the increase in muscle force further to only 34% in *Mstn*^{-/-}-OVL-HLF ($P = 0.0224$ for HLF effect, $P =$ non-significant for combined effect), thus, 42% less than in *Mstn*^{-/-}-OVL (558 mN versus 729 mN). Specific force did not change significantly (Figure 4E). These results suggest that force increase following overload was associated with the intensive ECM remodelling. Lack of myostatin provided no functional advantage for the overloaded muscle.

Effect of overload on muscle histology

Overload induced a massive appearance of fibres with internalized myonuclei, which is considered a marker of fibre regeneration following necrosis. This was seen in both genotypes irrespectively of concomitant halofuginone treatment (Figure 4F, $P < 0.0001$ for *WT* and $P = 0.0013$ for *Mstn*^{-/-}). In addition, we observed increased fibre size variability following overload for both genotypes (Figures 5A-C).

Effect of overload on muscle contractile phenotype

These above RNA analysis suggested that *Mstn*^{-/-} muscle may resist overload-induced fibre type conversion. Indeed, in *WT* muscle, overload substantially converted fibre types from fast glycolytic MHCIb expressing fibres towards slow oxidative MHCI ($P = 0.0093$) and fast oxidative MHCIa expressing fibres ($P = 0.0091$), (Figures 6A-C). Lack of myostatin, however, largely reduced overload triggered conversion towards MHCI fibres and MHCIa fibres. The effect of halofuginone on fibre-type conversion was only minor (Figures 6A-C).

Effect of overload on TGF-β signalling

RT-qPCR on RNA from *plantaris* muscle homogenates revealed strong increases in transcription for genes involved in TGF-β signalling following overload for *WT* mice and *Mstn*^{-/-} mice: *Tgfb1*, *Tgfb2*, *Tgfb2*, *Serpine1*

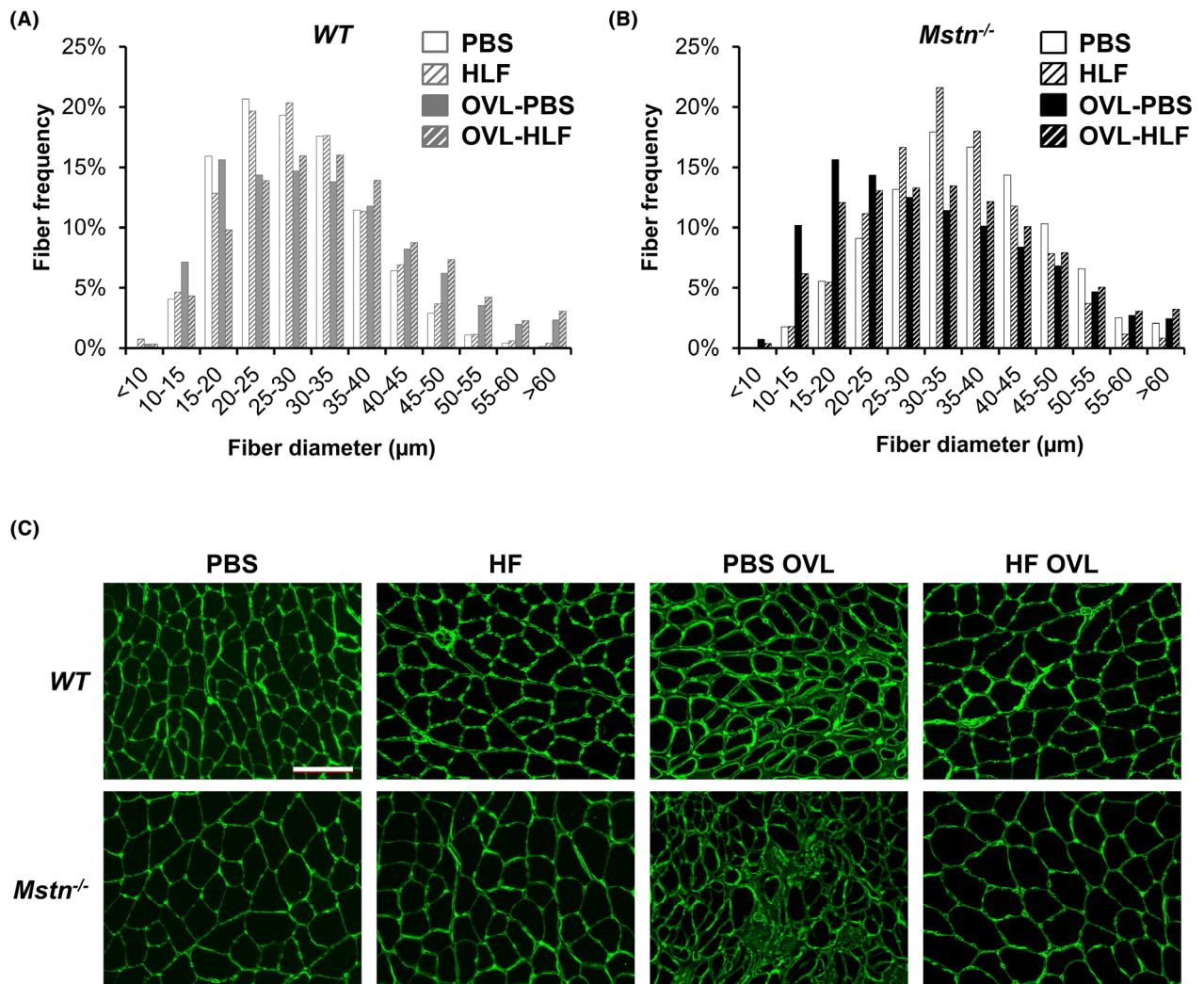


Figure 5. Overload effect on fibre diameter and fibrosis in WT and $Mstn^{-/-}$ mice following halofuginone treatment. Mice were treated as described in Figure 4. (A–B) Fibre size histograms of WT (A) and $Mstn^{-/-}$ (B) *plantaris* muscle fibres on mid-belly sections following immunostaining against collagen 1 ($n = 2000$ – 5000 fibres/group). (C) Fluorescent microscopic images following immunostaining against collagen 1 (green) of mid-belly transverse sections of *plantaris* muscles. Scale bar: 100 μm .

and *P21 genes* ($P < 0.05$ for all genes and genotypes), (Figure 7). We were unable to discriminate any effect of myostatin knockout or halofuginone on the expression of any of these genes.

Discussion

This study reveals unexpected findings regarding the role of muscle ECM that question current paradigms in skeletal muscle pathophysiology.

In WT mice, we reproduced previous findings on the chronic effects of surgical ablation of *plantaris* muscle

synergists; namely, an increase in muscle ECM deposition, in fibre size variation, in mean fibre cross-sectional area, in muscle mass and in maximal tetanic force, as well as many regenerated fibres and a shift towards a more oxidative muscle phenotype. The magnitude of these parameters is similar to those published previously, thereby validating our experimental setup [36,37,46]. The origin of increased ECM deposition can easily be explained, likely to be triggered by the severe muscle inflammation and the increased TGF- β signalling that is induced in *plantaris* muscle following surgical ablation of synergists as seen by us and others

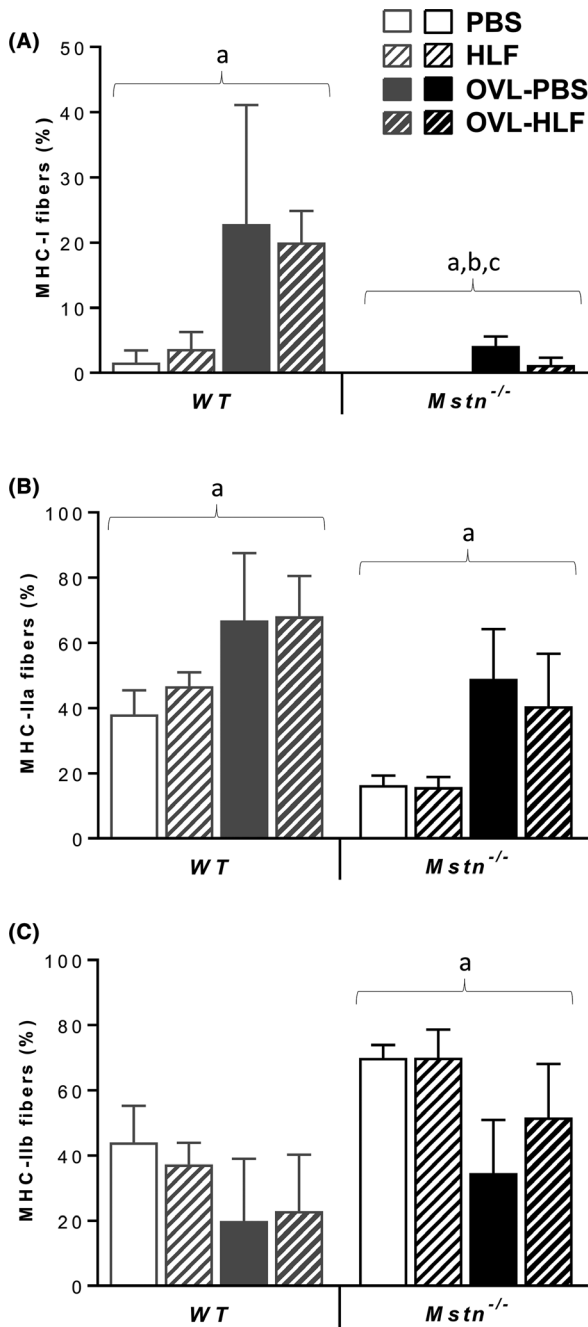


Figure 6. Overload effect on muscle fibre type composition in WT and *Mstn*^{-/-} mice following halofuginone treatment. Mice were treated as described in Figure 4. Immunostaining on *plantaris* muscle cross sections was performed against either MHC I fibres alone (A) or MHCIIa and MHCIIb fibres together (B, C), in which case unstained MHCIIa/IIb were excluded from quantification since they could either be MHC I or MHCIIx fibres. WT diagrams are in grey, *Mstn*^{-/-} diagrams are in black. Values are depicted as means \pm SD ($n = 3$ muscles/group). Two-way ANOVA test was performed. (A) Diagrams depict MHC I fibre-type distribution. WT diagram: ^a $P = 0.0093$ (effect of OVL). *Mstn*^{-/-} diagram: ^a $P = 0.0008$ (effect of OVL), ^b $P = 0.0219$ (effect of HLF) and ^c $P = 0.0219$ (combined effect of OVL and HLF). (B) Diagrams depict MHCIIa distribution. WT diagram: ^a $P = 0.0091$ (effect of OVL). *Mstn*^{-/-} diagram: ^a $P = 0.0023$ (effect of OVL). (C) Diagrams depict MHCIIb distribution. *Mstn*^{-/-} diagram: ^a $P = 0.006$ (effect of OVL).

skeletal muscle as previously observed in mouse models for muscular dystrophy [22–26]. Such “amelioration” of muscle histology by halofuginone, curiously, blunted the increase in muscle mass. Therefore, muscle ECM makes a non-negligible part of muscle mass and its proportion increases following overload, which was reduced by halofuginone. However, ECM deposition, is likely combined with increased extracellular water retention, as shown by [²³Na] MRS in dystrophic muscle [47,48], explaining the important increase on muscle wet weight following overload and the inhibition by concomitant treatment with halofuginone.

The increase in maximal force generation in response to overload was also blunted by halofuginone. Thus, tendencies for changes in ECM, muscle mass and muscle force correlated with each other, whereas these parameters did not correlate with myofibre size. Although we found an association between ECM remodelling and muscle force increase, we are lacking proof whether ECM remodelling is causative. Alternative explanations, such as load-induced increase in active contractile force, must be considered, although we did not observe changes in specific force generation. Of note, we here determined specific force of the whole *plantaris* muscle. However, in order to differentiate between respective contributions of the contractile apparatus *versus* ECM remodelling, force generation should be compared between skinned and non-skinned fibres. Therefore, studies of lateral force transmission would be required to dissect the effect of overload on active contraction, tensile strength and shearing.

Force transmission depends on the viscoelastic properties of the muscles, which in turn depends on its ECM

[33,34]. The functional effect of such ECM remodelling in this chronic overload model, however, remains unknown.

Here, we show that treatment with halofuginone reduced ECM deposition in overloaded muscles, while myofibre size increased. This result confirms the antifibrotic and promyogenic effect of halofuginone in

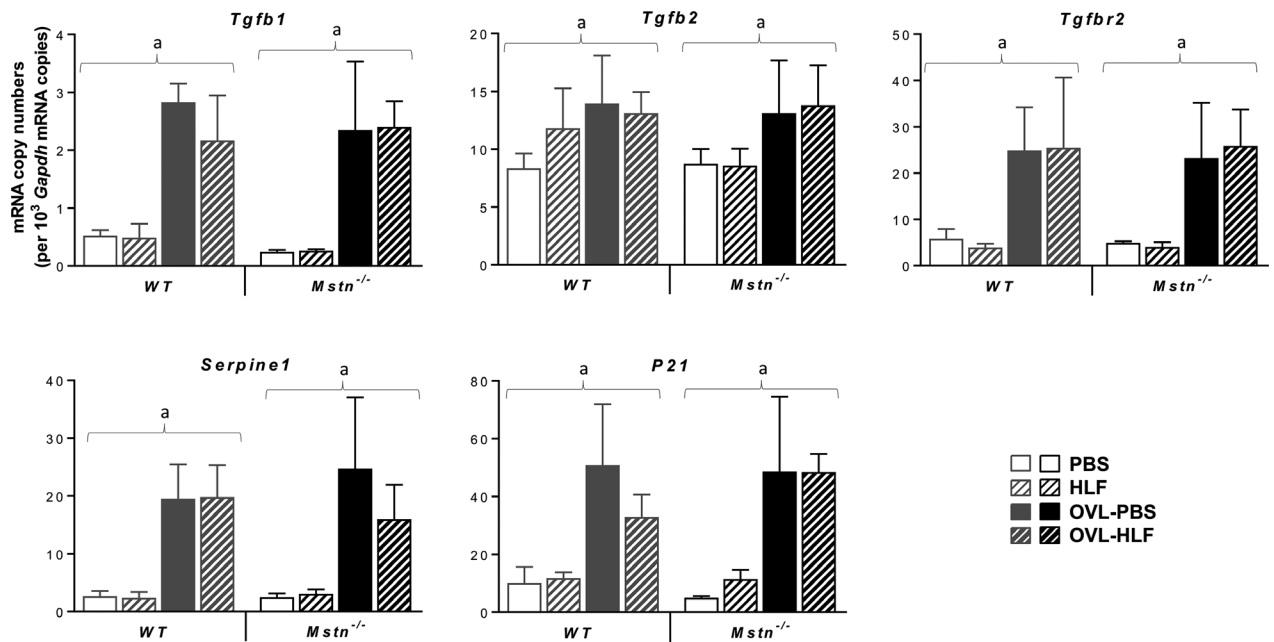


Figure 7. Effect of overload on the expression of TGF- β signalling components in WT and *Mstn*^{-/-} mice following halofuginone treatment. Mice were treated as described in Figure 4. Histograms depict the RT-qPCR results showing the relative mRNA copy numbers as expressed per 10E3 \times *Gapdh* mRNA copies in the *plantaris* muscle of WT (in grey) and *Mstn*^{-/-} (in black) mice, of TGF- β ligands *Tgfb1* and *Tgfb2*, TGF- β receptor *Tgfb2*, *Serpine1* and *P21*. WT diagrams are in grey, *Mstn*^{-/-} diagrams are in black. Values are depicted as means \pm SD ($n = 3$ -5/group). Two-way ANOVA test was performed.

composition. Weakened ECM is associated with force drop and decreased force transmission in Marfan syndrome and Ehlers-Danlos syndrome [49–52]. In healthy muscle, the endomysium does not contribute to tensile strength as its compliance is too large. However, its shear properties are pivotal for lateral force transmission, which exerts tension on tendons *via* perimysium and epimysium [53]. We suggest that overload-induced ECM remodelling changes passive muscle properties at the endomysial level, thereby increasing force transmission, a hypothesis that remains to be proven experimentally.

We also lack experimental proof, whether the hypertrophic effect of halofuginone on overloaded muscle fibres was direct or indirect. We did not find any hypertrophic response to halofuginone in non-overloaded WT muscles and there was no change in the expression of the TGF- β signalling target *P21*, suggesting that halofuginone acted more indirectly on muscle *via* inhibition of ECM remodelling.

We here compared the phenotype of WT to *Mstn*^{-/-} *plantaris* muscle, which had not yet been studied before. We found increased muscle mass, muscle fibre hypertrophy and hyperplasia, increased maximal tetanic force, decreased specific force and a shift from oxidative

fast fibres towards fast glycolytic fibres. These findings are in agreement with the expected phenotype from *Mstn* knockout and notably resemble the phenotype of *Mstn*^{-/-} *extensor digitorum longus* muscle, which, like *plantaris*, is also a fast muscle [54–56].

Ablation of synergistic muscles had different consequences for *Mstn*^{-/-} *plantaris* muscle and for WT controls. Although the increase in total muscle weight and force was similar, the proportional increase in these parameters was much lower in *Mstn*^{-/-} mice as compared to WT mice. Similar findings for muscle mass were seen in muscles from another mouse strain, the BEH mice [57], which also carry a loss-of-function mutation in *Mstn*. In BEH mice, however, maximal muscle force did not increase at all following overload, leading to a strong decrease in specific force [58]. Here, we found an inability of overloaded *Mstn*^{-/-} muscle to convert towards slow MHCII fibres and a decreased conversion towards fast MHCIIa fibres, while maintaining a higher number of fast glycolytic MHCIIb fibres. However, these findings do not explain the blunted force increase because a “fast” muscle phenotype would rather be expected to generate stronger force in comparison to the “slow” phenotype of the overloaded WT

muscle. Intriguingly, we observed a strong decrease in *Mstn*^{-/-} myofibre diameter following overload, which was mainly due to a strong increase in small fibres and not by loss of large fibres. Thus, in overloaded *Mstn*^{-/-} *plantaris*, maximal tetanic force increased despite a shift towards smaller fibre diameters.

Overload-induced de- and regeneration of myofibres was clearly visible by the increase in myofibres with internalized myonuclei and by the expression of developmental MHC isoforms. Previous studies have shown that regenerating muscle transiently also upregulates MHCIIb expression, however, we here found its mRNA message was downregulated. Since MHCIIb is only very transiently expressed, our analysis might have been too late, or maybe its upregulation was overruled by the effect of overload.

Interestingly, we did not find any difference in ECM remodelling between *Mstn*^{-/-} and control muscles following overload, if at all, ECM deposition tended to be stronger in *Mstn*^{-/-} muscle. This suggests that lack of myostatin may not have as much of an antifibrotic effect as previously suggested, if at all [17]. This view is supported by the findings that myostatin is not upregulated; in fact, myostatin is downregulated following overload. This also applies to dystrophic *mdx* mice proposing the notion that myostatin expression may be unrelated to ECM remodelling [59,60]. We show that halofuginone, in contrast to myostatin deficiency, did blunt ECM deposition and increased myofibre size in overloaded *Mstn*^{-/-} muscle. This further supports the notion that ECM remodelling would be independent of myostatin signalling and likely caused by increased TGF- β signalling. This also suggests that increased ECM deposition itself may be the cause of muscle fibre hypotrophy and that this outweighed the hypertrophic effect of myostatin deficiency.

We were surprised to find a downregulation of genes related to oxidative and mitochondrial metabolism as this stands in contrast to the conversion toward more oxidative fibre types. Our interpretation of these findings is that overload changed the overall composition of muscle tissue towards connective tissue, which is less metabolically active, as can also be seen by the even higher depletion of genes associated with the glycogen metabolic process (Figure 1).

Chronic muscle overload following ablation of synergistic muscles is widely used as a model for resistance training. However, we show here, as others have done

previously, that the mechanical stress of overload causes myofibre damage, inflammation, regeneration and ECM deposition, as well as conversion toward slow fibre types, which all are typical findings in muscular dystrophies [32–38]. Furthermore, TGF- β signalling is strongly induced following overload as well as in muscular dystrophies [34,61–64]. Interestingly, in DMD muscle, fibrosis starts at the muscle-tendon interphase, a site with the highest mechanical stress on the muscle fibres [12,65]. We therefore wondered whether fibrosis would represent a simple sequelae or a protective compensation, and whether we could extrapolate the findings of our study to muscular dystrophies in general. We would like to forward the daring hypothesis that muscle ECM remodelling in states of muscular dystrophies may improve force transmission, thereby lowering the required force output from the contractile portions of the muscle which ultimately might protect muscle fibres from further load-induced injury. If true, this would contradict the current rationale for therapeutic strategies aiming at the primary end-point of muscle fibrosis reduction. However, there are also several reports in the literature that would contradict our theory: (i) Blocking of TGF- β 1 signalling decreased fibrosis and reduced exercise-induced loss of muscle force in *mdx* mice [66]. (ii) Lateral force transmission was decreased in *mdx* mice [67]. (iii) Muscle compliance is increased, leading to aberrant mechanotransduction [68]. However, it remains unexplored to what degree endomysial fibrosis compensates for deficient transmembrane stability in lack of dystrophin, or whether ECM remodelling in DMD is a purely secondary and unrelated pathological response, which only bears negative consequences for muscle biomechanics. To address these questions, further work will be required, and we will repeat our experiments in *mdx* mice.

In summary, we here show that halofuginone blunts ECM deposition and stimulates hypertrophic myofibre growth following chronic mechanical overload of *plantaris* muscle; however, this reduces overall increase in muscle mass and force. Lack of myostatin does not convey any beneficial effect. In fact, overload of *Mstn*^{-/-} muscles induced values for fibre size, ECM deposition and muscle force that were not different from *WT* mice. We hypothesize that muscle ECM remodelling would be an important physiological response to mechanical stress and that this would be associated with the ability of the muscle to optimize force transmission.

Data Sharing and Data Accessibility

The raw data of this publication consisting of 24 datasets of Affymetrix Mouse Gene 1.0 ST Array readouts (CEL files) can be accessed freely at the GEO database under GSE127255, URL: <https://www.ncbi.nlm.nih.gov/geo/query/acc.cgi?acc=GSE127255>. Each experimental condition is represented by three biological replicates.

Acknowledgements

Financial support has been provided by ANR-Blanc Androgluco, the Association Française contre les Myopathies (AFM), MyoAge (EC 7th FP, contract 223576), MyoGrad International Graduate School for Myology (DRK 1631/1) and by the Deutsche Forschungsgemeinschaft (DFG; German Research Foundation) under Germany's Excellence Strategy – EXC-2049 – 390688087. We thank the genomics facility of the Simone Veil School of Health Sciences of the University of Versailles Saint-Quentin and Paris-Saclay for its logistic and technical support. Open access funding enabled and organized by Projekt DEAL.

Author Contributions

H. Amthor and M. Schuelke designed and supervised research; A. Stantzou, K. Relizani, C. Batot, A. Grassin and M. Schuelke analysed data; A. Stantzou, K. Relizani, S. Morales-Gonzalez and A. Ferry performed research; A. Stantzou and M. Schuelke prepared the figures; H. Amthor wrote the article. All authors read the manuscript and consented to its publication.

Ethical Approval

All procedures were done in accordance with national and European legislation, under the license 75-1102 (France).

Conflicts of Interests

The authors declare no conflict of interest.

References

- Lynch GS, Hinkle RT, Chamberlain JS, Brooks SV, Faulkner JA. Force and power output of fast and slow skeletal muscles from mdx mice 6–28 months old. *J Physiol* 2001; **535**(2): 591–600
- Relizani K, Mouisel E, Giannesini B, Hourdé C, Patel K, Morales Gonzalez S, et al. Blockade of ActRIIB signaling triggers muscle fatigability and metabolic myopathy. *Mol Ther* 2014; **22**(8): 1423–33
- Joe AWB, Yi L, Natarajan A, Le Grand F, So L, Wang J, et al. Muscle injury activates resident fibro/adipogenic progenitors that facilitate myogenesis. *Nat Cell Biol* 2010; **12**(2): 153–63
- Uezumi A, Fukada S, Yamamoto N, Takeda S, Tsuchida K. Mesenchymal progenitors distinct from satellite cells contribute to ectopic fat cell formation in skeletal muscle. *Nat Cell Biol* 2010; **12**(2): 143–52
- Dubowitz V. The muscular dystrophies. In: *Muscle disorders in childhood*. London: W. B. Saunders, 1995; 34–133
- Ohlendieck K, Swandulla D. Molecular pathogenesis of Duchenne muscular dystrophy-related fibrosis. *Pathology* 2017; **38**(1): 21–9
- Serrano AL, Muñoz-Cánoves P. Fibrosis development in early-onset muscular dystrophies: Mechanisms and translational implications. *Semin Cell Dev Biol* 2017; **64**: 181–90
- Lemos DR, Babaeijandaghi F, Low M, Chang C-K, Lee ST, Fiore D, et al. Nilotinib reduces muscle fibrosis in chronic muscle injury by promoting TNF-mediated apoptosis of fibro/adipogenic progenitors. *Nat Med* 2015; **21**(7): 786–94
- Marinkovic M, Fuoco C, Sacco F, Perpetuini AC, Giuliani G, Micarelli E, et al. Fibro-adipogenic progenitors of dystrophic mice are insensitive to NOTCH regulation of adipogenesis. *Life Sci Alliance* 2019; **2**(3): e201900437. Available from <https://www.life-science-alliance.org/content/2/3/e201900437>.
- Hogarth MW, Defour A, Lazarski C, Gallardo E, Diaz Manera J, Partridge TA, et al. Fibroadipogenic progenitors are responsible for muscle loss in limb girdle muscular dystrophy 2B. *Nat Commun* 2019; **10**(1): 2430
- Delaney K, Kasprzycka P, Ciemerych MA, Zimowska M. The role of TGF- β 1 during skeletal muscle regeneration. *Cell Biol Int* 2017; **41**(7): 706–15
- Chrzanowski SM, Baligand C, Willcocks RJ, Deol J, Schmalfuss I, Lott DJ, et al. Multi-slice MRI reveals heterogeneity in disease distribution along the length of muscle in Duchenne muscular dystrophy. *Acta Myol* 2017; **36**(3): 151–62
- Zhou L, Lu H. Targeting fibrosis in Duchenne muscular dystrophy. *J Neuropathol Exp Neurol*. 2010; **69**(8): 771–6
- Spinazzola JM, Kunkel LM. Pharmacological therapeutics targeting the secondary defects and downstream pathology of Duchenne muscular dystrophy. *Expert Opin Orphan Drugs*. 2016; **4**(11): 1179–94
- Walton KL, Johnson KE, Harrison CA. Targeting TGF- β mediated SMAD signaling for the prevention of fibrosis. *Front Pharmacol* 2017; **8**: 461

- 16 Zimowska M, Duchesnay A, Dragun P, Oberbek A, Moraczewski J, Martelly I. Immunoneutralization of TGFbeta1 improves skeletal muscle regeneration: effects on myoblast differentiation and glycosaminoglycan content. *Int J Cell Biol* 2009; 2009: 659372
- 17 Yousef H, Conboy MJ, Morgenthaler A, Schlesinger C, Bugaj L, Paliwal P, et al. Systemic attenuation of the TGF- β pathway by a single drug simultaneously rejuvenates hippocampal neurogenesis and myogenesis in the same old mammal. *Oncotarget* 2015; 6(14): 11959–78
- 18 Wagner KR. Muscle regeneration through myostatin inhibition. *Curr Opin Rheumatol* 2005; 17(6): 720–4
- 19 Zhu J, Li Y, Shen W, Qiao C, Ambrosio F, Lavasani M, et al. Relationships between transforming growth factor-beta1, myostatin, and decorin: implications for skeletal muscle fibrosis. *J Biol Chem*. 2007; 282(35): 25852–63
- 20 Li ZB, Zhang J, Wagner KR. Inhibition of myostatin reverses muscle fibrosis through apoptosis. *J Cell Sci*. 2012; 125(17): 3957–65
- 21 McGaha TL, Phelps RG, Spiera H, Bona C. Halofuginone, an inhibitor of type-I collagen synthesis and skin sclerosis, blocks transforming-growth-factor-beta-mediated Smad3 activation in fibroblasts. *J Invest Dermatol* 2002; 118(3): 461–70
- 22 Turgeman T, Hagai Y, Huebner K, Jassal DS, Anderson JE, Genin O, et al. Prevention of muscle fibrosis and improvement in muscle performance in the mdx mouse by halofuginone. *Neuromuscul Disord NMD*. 2008; 18(11): 857–68
- 23 Nevo Y, Halevy O, Genin O, Moshe I, Turgeman T, Harel M, et al. Fibrosis inhibition and muscle histopathology improvement in laminin-alpha2-deficient mice. *Muscle Nerve*. 2010; 42(2): 218–29
- 24 Bodanovsky A, Guttman N, Barzilai-Tutsch H, Genin O, Levy O, Pines M, et al. Halofuginone improves muscle-cell survival in muscular dystrophies. *Biochim Biophys Acta* 2014; 1843(7): 1339–47
- 25 Levi O, Genin O, Angelini C, Halevy O, Pines M. Inhibition of muscle fibrosis results in increases in both utrophin levels and the number of revertant myofibers in Duchenne muscular dystrophy. *Oncotarget*. 2015; 6(27): 23249–60
- 26 Barzilai-Tutsch H, Bodanovsky A, Maimon H, Pines M, Halevy O. Halofuginone promotes satellite cell activation and survival in muscular dystrophies. *Biochim Biophys Acta* 2016; 1862(1): 1–11
- 27 Ianuzzo CD, Gollnick PD, Armstrong RB. Compensatory adaptations of skeletal muscle fiber types to a long-term functional overload. *Life Sci* 1976; 19(10): 1517–23
- 28 Baldwin KM, Valdez V, Herrick RE, MacIntosh AM, Roy RR. Biochemical properties of overloaded fast-twitch skeletal muscle. *J Appl Physiol* 1982; 52(2): 467–72
- 29 Booth FW, Thomason DB. Molecular and cellular adaptation of muscle in response to exercise: perspectives of various models. *Physiol Rev* 1991; 71(2): 541–85
- 30 Roy RR, Edgerton VR. Response of mouse plantaris muscle to functional overload: comparison with rat and cat. *Comp Biochem Physiol A Physiol* 1995; 111(4): 569–75
- 31 Bodine SC, Baar K. Analysis of skeletal muscle hypertrophy in models of increased loading. *Methods Mol Biol Clifton NJ* 2012; 798: 213–29
- 32 Armstrong RB, Marum P, Tullson P, Saubert CW. Acute hypertrophic response of skeletal muscle to removal of synergists. *J Appl Physiol* 1979; 46(4): 835–42
- 33 Di Pasquale DM, Cheng M, Billich W, Huang SA, van Rooijen N, Hornberger TA, et al. Urokinase-type plasminogen activator and macrophages are required for skeletal muscle hypertrophy in mice. *Am J Physiol Cell Physiol* 2007; 293(4): C1278–1285
- 34 White JP, Reecy JM, Washington TA, Sato S, Le ME, Davis JM, et al. Overload-induced skeletal muscle extracellular matrix remodelling and myofibre growth in mice lacking IL-6. *Acta Physiol Oxf Engl* 2009; 197(4): 321–32
- 35 McCarthy JJ, Mula J, Miyazaki M, Erfani R, Garrison K, Farooqui AB, et al. Effective fiber hypertrophy in satellite cell-depleted skeletal muscle. *Dev Camb Engl* 2011; 138(17): 3657–66
- 36 Joanne P, Hourdé C, Ochala J, Caudéran Y, Medja F, Vignaud A, et al. Impaired adaptive response to mechanical overloading in dystrophic skeletal muscle. *PLoS One* 2012; 7(4): e35346
- 37 Ferry A, Schuh M, Parlakian A, Mgrditchian T, Valnaud N, Joanne P, et al. Myofiber androgen receptor promotes maximal mechanical overload-induced muscle hypertrophy and fiber type transition in male mice. *Endocrinology* 2014; 155(12): 4739–48
- 38 Mendias CL, Schwartz AJ, Grekin JA, Gumucio JP, Sugg KB. Changes in muscle fiber contractility and extracellular matrix production during skeletal muscle hypertrophy. *J Appl Physiol Bethesda Md* 1985 2017; 122(3): 571–9
- 39 McPherron AC, Lawler AM, Lee S-J. Regulation of skeletal muscle mass in mice by a new TGF-p superfamily member. *Nature* 1997; 387(6628): 83–90
- 40 Kuehn H, Liberzon A, Reich M, Mesirov JP. Using GenePattern for gene expression analysis. *Curr Protoc Bioinforma* 2008; <https://doi.org/10.1002/0471250953.bi0712s22> (accessed at Sept 2015).
- 41 Huang DW, Sherman BT, Lempicki RA. Systematic and integrative analysis of large gene lists using DAVID bioinformatics resources. *Nat Protoc* 2008; 4(1): 44–57

- 42 Metsalu T, Vilo J. ClustVis: a web tool for visualizing clustering of multivariate data using Principal Component Analysis and heatmap. *Nucleic Acids Res* 2015; **43**(W1): W566–70
- 43 Pfaffl MW. A new mathematical model for relative quantification in real-time RT-PCR. *Nucleic Acids Res* 2001; **29**(9): 45e–45
- 44 Benjamini Y. Discovering the false discovery rate. *J Royal Stat Soc* 2010; **72**: 405–16
- 45 Welle S, Cardillo A, Zanche M, Tawil R. Skeletal muscle gene expression after myostatin knockout in mature mice. *Physiol Genomics* 2009; **38**(3): 342–50
- 46 Fajardo VA, Rietze BA, Chambers PJ, Bellissimo C, Bombardier E, Quadrilatero J, et al. Effects of sarcolipin deletion on skeletal muscle adaptive responses to functional overload and unload. *Am J Physiol-Cell Physiol* 2017; **313**(2): C154–61
- 47 Weber M-A, Nagel AM, Wolf MB, Jurkat-Rott K, Kauczor H-U, Semmler W, et al. Permanent muscular sodium overload and persistent muscle edema in Duchenne muscular dystrophy: a possible contributor of progressive muscle degeneration. *J Neurol* 2012; **259**(11): 2385–92
- 48 Kushnir T, Knubovets T, Itzhak Y, Eliav U, Sadeh M, Rapoport L, et al. In vivo ^{23}Na NMR studies of myotonic dystrophy. *Magn Reson Med* 1997; **37**(2): 192–6
- 49 Percheron G, Fayet G, Ningler T, Le Parc J-M, Denot-Ledunois S, Leroy M, et al. Muscle strength and body composition in adult women with Marfan syndrome. *Rheumatology* 2007; **46**(6): 957–62
- 50 Miller G, Neilan M, Chia R, Gheryani N, Holt N, Charbit A, et al. ENU mutagenesis reveals a novel phenotype of reduced limb strength in mice lacking fibrillin 2. *PLoS One* 2010; **5**(2): e9137
- 51 Huijing PA, Voermans NC, Baan GC, Busé TE, van Engelen BGM, de Haan A. Muscle characteristics and altered myofascial force transmission in tenascin-X-deficient mice, a mouse model of Ehlers-Danlos syndrome. *J Appl Physiol* 2010; **109**(4): 986–95
- 52 Voermans NC, Altenburg TM, Hamel BC, de Haan A, van Engelen BG. Reduced quantitative muscle function in tenascin-X deficient Ehlers-Danlos patients. *Neuromuscul Disord* 2007; **17**(8): 597–602
- 53 Purslow Peter P. The structure and role of intramuscular connective tissue in muscle function. *Front Physiol* 2020; **11**: <https://doi.org/10.3389/fphys.2020.00495>. Available from: <https://www.frontiersin.org/articles/10.3389/fphys.2020.00495/full>.
- 54 Mendias CL, Marcin JE, Calderon DR, Faulkner JA. Contractile properties of EDL and soleus muscles of myostatin-deficient mice. *J Appl Physiol Bethesda Md* 1985 2006; **101**(3): 898–905
- 55 Amthor H, Macharia R, Navarrete R, Schuelke M, Brown SC, Otto A, et al. Lack of myostatin results in excessive muscle growth but impaired force generation. *Proc Natl Acad Sci U S A* 2007; **104**(6): 1835–40
- 56 Mouisel E, Relizani K, Mille-Hamard L, Denis R, Hourdé C, Agbulut O, et al. Myostatin is a key mediator between energy metabolism and endurance capacity of skeletal muscle. *Am J Physiol Regul Integr Comp Physiol* 2014; **307**(4): R444–454
- 57 Kilikevicius A, Bungler L, Lionikas A. Baseline muscle mass is a poor predictor of functional overload-induced gain in the mouse model. *Front Physiol* 2016; **7**: 534
- 58 Minderis P, Kilikevicius A, Baltusnikas J, Alhindi Y, Venckunas T, Bungler L, et al. Myostatin dysfunction is associated with reduction in overload induced hypertrophy of soleus muscle in mice. *Scand J Med Sci Sports* 2016; **26**(8): 894–901
- 59 Mariot V, Joubert R, Hourdé C, Féasson L, Hanna M, Muntoni F, et al. Downregulation of myostatin pathway in neuromuscular diseases may explain challenges of anti-myostatin therapeutic approaches. *Nat Commun* 2017; **8**(1): 1859
- 60 Pérez-Schindler J, Esparza MC, McKendry J, Breen L, Philp A, Schenk S. Overload-mediated skeletal muscle hypertrophy is not impaired by loss of myofiber STAT3. *Am J Physiol Cell Physiol* 2017; **313**(3): C257–61
- 61 Ishitobi M, Haginoya K, Zhao Y, Ohnuma A, Minato J, Yanagisawa T, et al. Elevated plasma levels of transforming growth factor beta1 in patients with muscular dystrophy. *NeuroReport* 2000; **11**(18): 4033–5
- 62 Hartel JV, Granchelli JA, Hudecki MS, Pollina CM, Gosselin LE. Impact of prednisone on TGF-beta1 and collagen in diaphragm muscle from mdx mice. *Muscle Nerve* 2001; **24**(3): 428–32
- 63 Andreetta F, Bernasconi P, Baggi F, Ferro P, Oliva L, Arnoldi E, et al. Immunomodulation of TGF-beta 1 in mdx mouse inhibits connective tissue proliferation in diaphragm but increases inflammatory response: implications for antifibrotic therapy. *J Neuroimmunol*. 2006; **175**(1–2): 77–86
- 64 Zhou L, Porter JD, Cheng G, Gong B, Hatala DA, Merriam AP, et al. Temporal and spatial mRNA expression patterns of TGF-beta1, 2, 3 and TbetaRI, II, III in skeletal muscles of mdx mice. *Neuromuscul Disord NMD* 2006; **16**(1): 32–8
- 65 Petrof BJ, Shrager JB, Stedman HH, Kelly AM, Sweeney HL. Dystrophin protects the sarcolemma from stresses developed during muscle contraction. *Proc Natl Acad Sci* 1993; **90**(8): 3710–4
- 66 Taniguti APT, Pertille A, Matsumura CY, Santo Neto H, Marques MJ. Prevention of muscle fibrosis and myonecrosis in mdx mice by suramin, a TGF- β 1 blocker. *Muscle Nerve* 2011; **43**(1): 82–7
- 67 Ramaswamy KS, Palmer ML, van der Meulen JH, Renoux A, Kostrominova TY, Michele DE, et al. Lateral transmission of force is impaired in skeletal muscles of dystrophic mice and very old rats. *J Physiol* 2011; **589**(5): 1195–208

68 Kumar A, Khandelwal N, Malya R, Reid MB, Boriek AM. Loss of dystrophin causes aberrant mechanotransduction in skeletal muscle fibers. *FASEB J Off Publ Fed Am Soc Exp Biol* 2004; **18**(1): 102–13

Supporting information

Additional Supporting Information may be found in the online version of this article at the publisher's web-site:

Figure S1. Correlation between mRNA copy number fold changes measured with RNA-microarray and RT-qPCR for representative up- and down-regulated genes. CN, copy numbers (copy numbers were normalized to *GAPDH* mRNA copy numbers for low-copy genes and to 18S rRNA copy numbers for high-copy genes); **Mstn**, myostatin; **SI**, signal intensity normalized by the Agilent MAS 5.0 algorithm; **WT**, wild-type

Figure S2. Relative regulation after overload of transcript numbers of genes encoding the various myosin heavy and light chains. (A) Heat map and clustergram of various heavy and light myosin isoforms. Copy numbers of the genes that encode the myosin isoforms Myh3, Myh8, and Myl4 [1]. These three myosin isoforms characteristically contribute to the early and developmental forms of myosin and are highlighted by

red arrows. These isoforms are clearly upregulated after overload. (B) Principal component analysis in two dimensions (PCA 2D) of the four experimental conditions with 6 biological replicates. For PCA 2D, original values were $\ln(x)$ -transformed and the unit variance scaling was applied to rows; singular value decomposition (SVD) with imputation was used to calculate principal components. X- and Y-axes show principal components 1 and 2 that explain the indicated total variance. Prediction ellipses are such that with probability 0.95, a new observation from the same group will fall inside the ellipse. $N = 24$ data points. The exact list of genes and their expression differences are provided in Table S1.

Table S1. Up- and downregulated genes with an FDR below 0.01. Comparison WT overload vs. WT no overload (WT_noovld vs. WT_ovld) and comparison between *Mstn*^{-/-} overload vs. WT overload (Mstn_ovld vs. WT_ovld).

Table S2. Oligonucleotide primer sequences used for the RT-qPCR assays on Figure 7.

Received 18 December 2019

Accepted after revision 28 July 2020

Published online Article Accepted on 9 August 2020